

# Mass transfer and tidally tilted pulsation in the Algol-type system TZ Dra

F. Kahraman Aliçavuş<sup>1,2</sup>\*, G. Handler,<sup>3</sup> F. Aliçavuş,<sup>1,2</sup> P. De Cat<sup>4</sup>, T. R. Bedding<sup>5,6</sup>, P. Lampens,<sup>4</sup> Ö. Ekinci,<sup>1,2</sup> D. Gümüş<sup>7</sup> and F. Leone<sup>8,9</sup>

<sup>1</sup>Faculty of Sciences and Arts, Physics Department, Çanakkale Onsekiz Mart University, 17100 Canakkale, Turkey

<sup>2</sup>Astrophysics Research Center and Ulupınar Observatory, Çanakkale Onsekiz Mart University, TR-17100 Canakkale, Turkey

<sup>3</sup>Nicolaus Copernicus Astronomical Center, Polish Academy of Sciences, Bartycka 18, PL-00-716 Warsaw, Poland

<sup>4</sup>Royal Observatory of Belgium, Ringlaan 3, B-1180 Brussel, Belgium

<sup>5</sup>Sydney Institute for Astronomy (SfA), School of Physics, University of Sydney, Camperdown NSW 2006, Australia

<sup>6</sup>Stellar Astrophysics Centre, Department of Physics and Astronomy, Aarhus University, Ny Munkegade 120, DK-8000 Aarhus C, Denmark

<sup>7</sup>Institute of Graduate Studies in Science, Programme of Astronomy and Space Sciences, Istanbul University, 34116 Beyazıt, Istanbul, Turkey

<sup>8</sup>Dipartimento di Fisica e Astronomia, Sezione Astrofisica, Università di Catania, Via S. Sofia 78, I-95123 Catania, Italy

<sup>9</sup>INAF, Osservatorio Astrofisico di Catania, Via S. Sofia 78, I-95123 Catania, Italy

Accepted 2021 November 30. Received 2021 November 30; in original form 2021 September 27

## ABSTRACT

Oscillating eclipsing Algols (oEAs) are remarkable systems that allow us to determine accurate fundamental stellar parameters (mass, radius) and probe the stellar interiors through pulsations. TZ Dra is an oEA system containing a  $\delta$  Scuti component. To examine particular characteristics of such close systems including pulsations and mass transfer, we present a detailed photometric and spectroscopic study of TZ Dra. With the analysis of high-resolution spectra, the orbital parameters were determined by the radial velocity analysis and the atmospheric parameters were derived for the primary component. The binary modelling and the pulsational frequency analysis was carried out using the *Transiting Exoplanet Survey Satellite* data set. The  $H\alpha$  line profiles show the signature of mass transfer from the cool to the hot binary component. The conclusion of mass transfer/mass-loss in the system was supported by the analysis of the orbital period changes. As a result, it was found that there is  $3.52 \times 10^{-9} M_{\odot} \text{ yr}^{-1}$  mass-loss from the system most probably through the hotspot and stellar winds. Additionally, most pulsation frequencies originating from the primary component were found to be spaced by harmonics of the orbital frequencies in particular, 12 doublets spaced by  $2f_{\text{orb}}$  were detected from which we infer that this star is a tidally tilted pulsator. A mean p-mode frequency spacing of  $\approx 7.2 \text{ d}^{-1}$  was found as well.

**Key words:** stars: atmospheres – binaries: eclipsing – stars: fundamental parameters – stars: individual: TZ Dra – stars: variables:  $\delta$  Scuti.

## 1 INTRODUCTION

A significant fraction ( $\sim 70$  per cent) of stars in our Galaxy is assumed to be a member of binary or multiple systems (Sana & Evans 2011; Alfonso-Garzón et al. 2014; Moe & Di Stefano 2017). A special group of binary systems is the eclipsing binaries. As the eclipsing binary stars are particular tools for the accurate determination of the fundamental stellar parameters such as mass ( $M$ ) and radius ( $R$ ), they are among the most studied stellar systems.

There are also some extremely spectacular eclipsing binaries that consist of at least one pulsating star. These kinds of systems allow us to probe the stellar interiors through the study of pulsation frequencies occurring in the inner part of the oscillating binary component(s). Obtaining precise fundamental stellar parameters and having information about the stellar interior are certainly important and provides us powerful tools to check the validity of present stellar structure models and compare evolutionary models for single stars and stars in binary systems. Therefore, most studies

have been carried out about these objects for decades (e.g. Joergensen & Gronbech 1978; Broglia & Conconi 1984; Soyduğan et al. 2003; da Silva et al. 2014; Steindl, Zwintz & Bowman 2021).

Different kinds of high and intermediate-mass main-sequence oscillating stars like  $\beta$  Cephei,  $\delta$  Scuti, and  $\gamma$  Doradus can be components of eclipsing binaries (Lampens 2021; Southworth 2021). However, the number of eclipsing binaries with  $\delta$  Scuti components is the largest compared to other groups of main-sequence pulsating stars in eclipsing binaries (Kahraman Aliçavuş et al. 2017; Liakos & Niarchos 2017) because of their relatively shorter pulsation period and lower oscillation amplitude they are easier to detect. The  $\delta$  Scuti stars are  $A - F$  type, dwarf to giant, pulsating variables which exhibit pulsations with frequencies higher than  $5 \text{ d}^{-1}$  (Breger 2000; Balona & Dziembowski 2011; Bowman & Kurtz 2018; Murphy et al. 2019). Their oscillations are thought to be excited by the  $\kappa$  mechanism operating in the He ionization zone (Baker & Kippenhahn 1962). The  $\delta$  Scuti stars are located in the lower part of the classical Cepheid instability strip and they show pulsations in pressure (p) and gravity (g) modes which give information about different parts of the stellar interior.

\* E-mail: filizkahraman01@gmail.com, filizkahraman@comu.edu.tr

The first discoveries of  $\delta$  Scuti stars in eclipsing binary systems were presented in the beginning of the 1970s (Tempesti 1971). Since that time, the number of known  $\delta$  Scuti stars in eclipsing binaries has been increased. Significant attempts to find new candidates of this kind of systems were done by Mkrтчian et al. (2002, 2005) and Soyduđan et al. (2006). Soyduđan et al. (2006) gave a list of possible candidates by searching for eclipsing binaries positioned inside the  $\delta$  Scuti instability strip. Some new  $\delta$  Scuti stars in eclipsing binaries were discovered by the investigation of the candidate stars given in this list (e.g. Sumter & Beaky 2007; Soyduđan et al. 2008, 2011). The current number of the eclipsing binary  $\delta$  Scuti stars is around 90 in the latest published catalogue (Kahraman Aliçavuş et al. 2017). In recent years, this number is dramatically growing thanks to the high-precision data provided by the space telescopes such as *Convection Rotation and Planetary Transits* (Baglin et al. 2006), *Kepler* (Borucki et al. 2010), and *Transiting Exoplanet Survey Satellite* (*TESS*; Ricker et al. 2014). In addition to revealing the new eclipsing binary  $\delta$  Scuti stars, space telescopes also uncovered some new properties of these systems. For example, the first observational proof of  $\delta$  Scuti type pulsations in only one hemisphere of the pulsating component of a close binary was discovered with *TESS* data (Handler et al. 2020). Afterwards, a similar object was also found in an eclipsing binary (Rappaport et al. 2021). It was shown that in these close binaries the oscillation axis of the pulsating binary component is aligned with the tidal axis and hence the star exhibits pulsations more effectively on one of its hemisphere (Kurtz et al. 2020; Rappaport et al. 2021). These variables are now dubbed ‘single-sided pulsators’ (Handler et al. 2020) or, more general, tidally tilted pulsators (Fuller et al. 2020). As *TESS* observed almost the entire sky (Ricker et al. 2015), it has supplied sufficient data which help us to deeply understand the nature of stars like single-sided pulsators. *TESS* also observed a lot of known eclipsing binaries with  $\delta$  Scuti stars which had only ground-based photometric data of much lower precision until now. One of these systems is TZ Dra.

TZ Dra is an eclipsing binary system with a spectral type of A7 V (Herbig 1960; Faulkner 1986). Its pulsational characteristics were first revealed by Mkrтчian et al. (2005). They found that the system exhibits a  $\sim 28$  min oscillation and classified the primary (hot) binary component as a  $\delta$  Scuti star. Pulsating stars in eclipsing Algols are called ‘oscillating eclipsing Algol (oEA)’ (Mkrтчian et al. 2004). TZ Dra is also an oEA system with an orbital period of 0.8660307 d (Kreiner 2004). The oEAs are substantial systems to trace the effects of mass transfer and/or mass-loss to pulsations. In these Algol-type systems, mass is transferred from the evolved cool component to the pulsating hot component (Kopal 1955). It was shown that mass transfer affects the pulsations (Mkrтчian et al. 2004; Rodríguez et al. 2004). The effect of mass transfer in Algols can be revealed by following different features of the stellar spectra. Mass transfer can show itself as absorptions and/or emissions in  $H\alpha$  lines (Vesper, Honeycutt & Hunt 2001; Soyduđan et al. 2007). To investigate the effect/impact of mass transfer and/or mass-loss on pulsations in oEA systems, TZ Dra is a valuable system. Therefore, we performed a detailed analysis of TZ Dra using its high-quality *TESS* data in combination with newly acquired high-resolution spectra.

We organize the study as follows. In Section 2, the information about the observational data is given. The radial velocity measurements and their analysis are introduced in Section 3. In Sections 4 and 5, we present the spectral analysis and the binary modelling, respectively. The examination of the structure of the system’s  $H\alpha$  line is given in Section 6. The orbital period changes and the time-series analysis are introduced in Sections 7 and 8, respectively. In the final section, Section 9, discussion and conclusions are presented.

## 2 OBSERVATIONAL DATA

In our investigation, we used *TESS* data and obtained high-resolution spectra for TZ Dra.

*TESS* originally was designed to identify new exoplanets in bright stars ( $I_c < 13$ ). It was launched in 2018 April and until now *TESS* has observed almost entire of the sky. The *TESS* data have been taken with 2-min short cadence (SC) and 30-min long cadence (LC; Ricker et al. 2015) during the nominal mission (first 2 yr). Observations were done in 26 partly overlapping sectors of  $24^\circ \times 96^\circ$  that were observed for about 27 d each. Since the start of the extended mission in 2020 July, observations were done in a similar way but the cadence of the LC data has been increased to one observation every 10 min and a new 20-s cadence has been introduced. The *TESS* data are released in the Barbara A. Mikulski Archive for Telescopes (MAST).<sup>1</sup> For TZ Dra, only the LC data of sector 14 and SC data of sectors 25, 26 are available in the MAST. Simple Aperture Photometry flux of both high level science product LC and SC *TESS* data were taken from the MAST and used in the study.

The spectroscopic data were obtained using the High Efficiency and Resolution Mercator Échelle spectrograph (HERMES). The HERMES is attached to the 1.2-m Mercator telescope at the Roque de los Muchachos Observatory at La Palma, Spain. The spectrograph has a resolving power of 85 000 and it provides spectra in a spectral range from 377 to 900 nm (Raskin et al. 2011). For TZ Dra, we gathered 36 HERMES spectra between 2020 May and September. The spectra were taken at different epochs to get spectra spread over the orbital period of TZ Dra. The signal-to-noise (S/N) ratio of these spectra ranges from 60 to 100 and has an average of 83.

In this study, the *TESS* photometric data and HERMES spectra were used for the radial velocity analysis, binary modelling, the determination of the atmospheric parameters such as effective temperature ( $T_{\text{eff}}$ ), surface gravity ( $\log g$ ), microturbulence velocity ( $\xi$ ) and also projected rotational velocity ( $v \sin i$ ) of the system and time-series analysis.

## 3 RADIAL VELOCITY ANALYSIS

To accurately determine the fundamental stellar parameters of system, binary modelling should be done with the radial velocity ( $v_r$ ) measurements in addition to photometric data. Therefore, before performing the binary modelling we obtained the  $v_r$  data of the binary components. In this study, to measure the  $v_r$  values we used a synthetic spectrum that was generated considering the spectral type and an estimated  $v \sin i$  value ( $80 \text{ km s}^{-1}$ ) of TZ Dra. The initial  $v \sin i$  was determined by profile fitting. By using a synthetic spectrum, which has a similar spectral type and  $v \sin i$ , possible errors in the radial velocity measurements were decreased. The  $v_r$  values were obtained utilizing the FXCOR task of the IRAF<sup>2</sup> program package (Tody 1986). This task uses the cross-correlation technique that compares one spectrum to a template spectrum with a known velocity and zero redshift to find the redshift and velocity dispersion of the system under investigation to measure  $v_r$  values. As a result of our analysis, as we did not find a secondary peak in the cross-correlation profiles, we could only measure the  $v_r$  values of the primary component. The resulting  $v_r$  measurements are listed in Table A1.

The  $v_r$  analysis was carried out using the `rvfit` code<sup>3</sup> which is suitable for the  $v_r$  analysis of single and double-lined binary systems.

<sup>1</sup><https://mast.stsci.edu>

<sup>2</sup><http://iraf.noao.edu/>

<sup>3</sup><http://www.cefa.es/people/riglesias/rvfit.html>

**Table 1.** The results of the radial velocity analysis. <sup>a</sup> represents the fixed parameters.

Parameters	Value
$P$ (d)	$0.8660310^a$
$T_0$ (HJD)	$2452500.63606 \pm 0.00004$
$e$	$0.0^a$
$\omega$ (deg)	$90^a$
$\gamma$ ( $\text{km s}^{-1}$ )	$-25.02 \pm 0.11$
$K_1$ ( $\text{km s}^{-1}$ )	$90.90 \pm 0.20$
$a_1 \sin i$ ( $R_\odot$ )	$1.555 \pm 0.003$
$f(m_1, m_2)$ ( $M_\odot$ )	$0.0674 \pm 0.0004$

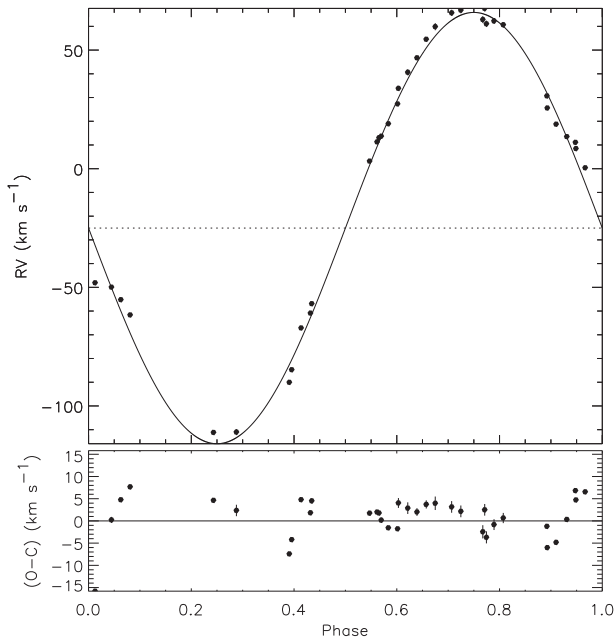


**Figure 1.** Upper panel: Theoretical (solid line) fit to the  $v_r$  measurements (dots). Lower panel: residuals.

First, an initial analysis was performed by fixing the orbital period of the system as  $0.8660307 \pm 0.0000010$  d (Kreiner 2004) and the periastron passage time ( $T_o$ ), the velocity of mass centre ( $V_\gamma$ ), the amplitude of the  $v_r$  curve ( $K$ ), argument of periastron ( $\omega$ ), orbital eccentricity ( $e$ ), and the projected semimajor axis ( $a \sin i$ ) parameters were searched for. As the  $e$  value was found to be 0 in the first a few iterations, this value and also the  $\omega$  parameter were assumed to be 0 and 90 deg, respectively, in the further analysis. After we approached the final values of the parameters the orbital period was investigated as well. In conclusion, we obtained the orbital parameters of TZ Dra that are given in Table 1. The best theoretical  $v_r$  fit to the  $v_r$  measurements is shown in Fig. 1.

#### 4 SPECTRAL ANALYSIS

In our radial-velocity analysis, no evidence of the cool (secondary) component spectrum was found in the cross-correlation function. Therefore, in our spectral analysis, we determined only the atmospheric parameters of the hot (primary) component. In any case, we used the spectra taken at close to 0.5 orbital phase where the secondary component is partially covered by the primary. In this way, we decreased the possible effect of the secondary component in

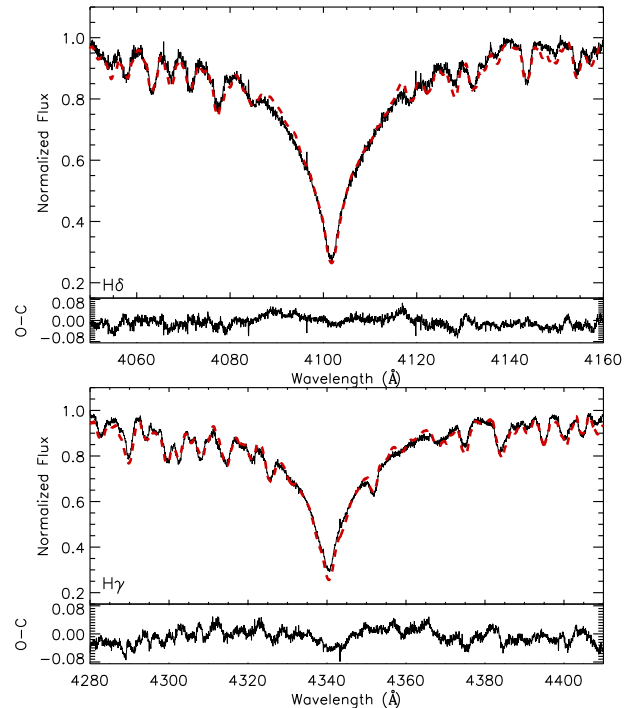


**Figure 2.** Theoretical hydrogen line fit (dashed line) to the observed H $\delta$  and H $\gamma$  lines. The differences between the observed (O) and calculated (C) spectra are shown below of each panel.

the spectra. Three spectra at around  $\sim 0.5$  phase (see Table A1) were chosen and combined to achieve a higher S/N ratio ( $\sim 165$ ) spectrum.

Using the combined spectrum, we first determined the initial  $T_{\text{eff}}$  value from the hydrogen line modelling. In this and next spectral analysis, the plane-parallel, hydrostatic, local thermodynamic equilibrium (LTE) ATLAS9 atmosphere models (Kurucz 1993) were used and the theoretical spectra were generated by using the SYNTHE code (Kurucz & Avrett 1981). In the hydrogen line analysis, we assumed solar abundance and fixed the  $\log g$  as 4.0 dex. These assumptions were made because the profile of the hydrogen lines is not affected by the metallicity and for the stars cooler than 8000 K there is a negligibly weak dependence on  $\log g$  (Smalley et al. 2002; Smalley 2005). Additionally, in the hydrogen line analysis, we only used H $\delta$  and H $\gamma$  lines because it is known that in Algol type systems due to the mass transfer effect there could be additional absorption and/or emission in the H $\alpha$  and H $\beta$  lines (Vesper et al. 2001; Soydugan et al. 2007). Those extra features in the hydrogen lines can be analysed after subtracting the theoretical hydrogen line profile. This examination is presented in Section 6.

In the hydrogen line analysis, several synthetic spectra were generated for a range of  $T_{\text{eff}}$  ( $\sim 7000$ – $8500$  K) in 100 K steps and they were fitted to the observed hydrogen lines. The best-fitting theoretical spectra were found considering the minimum  $\chi^2$  value (for more detail, see Catanzaro, Leone & Dall 2004). As a result of the analysis, we found a hydrogen  $T_{\text{eff}}$  values of  $7700 \pm 250$  K. The consistency of the theoretical hydrogen lines with the observations is demonstrated in Fig. 2.

To derive the  $\log g$  and  $\xi$  values and improve the  $T_{\text{eff}}$  value, we used the excitation/ionization-abundance relations which rely on the Boltzman and Saha equations. Taking into account the hydrogen-based  $T_{\text{eff}}$  we decided to use iron (Fe) lines because of their significant number at this  $T_{\text{eff}}$ . The method used in Kahraman Aliçavuş et al.

**Table 2.** The final atmospheric parameters and  $v \sin i$  value of the hot (primary) component star of TZ Dra.

$T_{\text{eff}}$ (K)	$\log g$ (cgs)	$\xi$ (km s $^{-1}$ )	$v \sin i$ (km s $^{-1}$ )
$8100 \pm 200$	$4.1 \pm 0.2$	$1.9 \pm 0.3$	$85 \pm 3$

**Table 3.** Abundances of individual elements of the primary star and Sun (Asplund et al. 2009). Number of the analysed spectral lines is given in third column.

Elements	Star abundance	Number of spectral parts	Solar abundance
$^6\text{C}$	$8.63 \pm 0.45$	1	$8.43 \pm 0.05$
$^{12}\text{Mg}$	$7.98 \pm 0.40$	4	$7.60 \pm 0.04$
$^{14}\text{Si}$	$6.97 \pm 0.36$	5	$7.51 \pm 0.03$
$^{20}\text{Ca}$	$6.48 \pm 0.31$	6	$6.34 \pm 0.04$
$^{21}\text{Sc}$	$3.37 \pm 0.41$	3	$3.15 \pm 0.04$
$^{22}\text{Ti}$	$4.91 \pm 0.34$	17	$4.95 \pm 0.05$
$^{23}\text{V}$	$4.15 \pm 0.42$	2	$3.93 \pm 0.08$
$^{24}\text{Cr}$	$5.57 \pm 0.35$	10	$5.64 \pm 0.04$
$^{25}\text{Mn}$	$5.02 \pm 0.33$	5	$5.43 \pm 0.05$
$^{26}\text{Fe}$	$7.37 \pm 0.21$	40	$7.50 \pm 0.04$
$^{28}\text{Ni}$	$6.18 \pm 0.38$	5	$6.22 \pm 0.04$
$^{38}\text{Sr}$	$2.71 \pm 0.45$	1	$2.87 \pm 0.07$
$^{56}\text{Ba}$	$2.39 \pm 0.42$	2	$2.18 \pm 0.07$

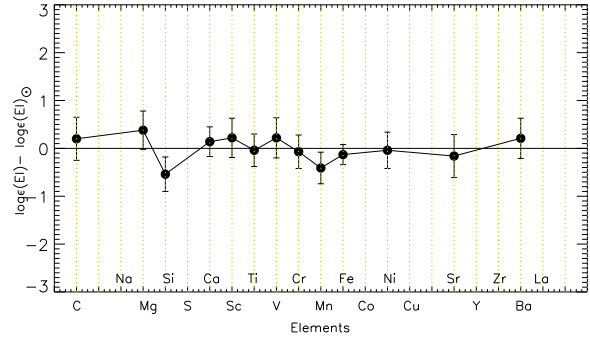
(2016) was applied in the same way in this study. First, the Fe lines were chosen from the line list of Kurucz<sup>4</sup> and their corresponding abundances were derived for a  $T_{\text{eff}}$ ,  $\log g$ , and  $\xi$  range with a step of 100 K, 0.1 dex, and 0.1 km s $^{-1}$ , respectively. The spectrum synthesis method was used in the analysis. It is known that for the correct atmospheric parameters, for different excitation/ionization potential one should get the same abundances as described by Kahraman Aliçavuş et al. (2016). In this way, the atmospheric parameters of the hot (primary) component of TZ Dra were obtained. The derived parameters are given in Table 2.

After we determined the atmospheric parameters, we derived the chemical abundances by taking these parameters as input and using the Kurucz line list. In this analysis, the abundances of the individual elements were adjusted until the minimum in the difference between the calculated and observed spectra was found. During this analysis, the  $v \sin i$  parameter was also searched for. The abundances of the chemical elements are listed in Table 3, while the  $v \sin i$  is given in Table 2. The chemical abundances distribution is also illustrated in Fig. 3. The consistency between the resulting synthetic and the observed combined spectrum is shown in Fig. 4.

The errors in the atmospheric parameters were estimated considering the 5 per cent difference in the used relations in the analysis. Additionally, the uncertainties in the chemical abundances were calculated taking into account the effects of the errors in the input parameters and S/N ratio as described by Kahraman Aliçavuş et al. (2016).

## 5 BINARY MODELLING

In order to derive the orbital and the fundamental stellar parameters of TZ Dra, we modelled the binary light curve. First, all the available TESS data were taken into account to check whether it changes from one sector to another. Because of the possible existence of spots on

**Figure 3.** The chemical abundance distribution of the primary component of TZ Dra. The solar abundance was taken from Asplund et al. (2009).

the surface of component(s), the flux level of the binary light curve during non-eclipsing phases could differ from one sector to another. These differences never affect the binary parameters, but only change the position of the spot on the surface of component(s). In the data of TZ Dra, no significant variation was found between the level of the out of eclipse brightness in the two sectors. Therefore, in the binary modelling we used both sector 25 and 26 data.

The pulsations in the system do not deeply affect the orbital/geometrical variation of TZ Dra. However, the dominant pulsations frequencies<sup>5</sup> were cleaned from the light curve rather than multiples of orbital period by performing a preliminary Fourier analysis with PERIOD04 (Lenz & Breger 2005, see section 8.2 for a more detailed description). The remaining data were first phased, normalized, and then binned to make them usable for the binary modelling with the Wilson–Devinney code (Wilson & Devinney 1971).

In this analysis, we used the findings of the previous binary modelling (Liakos & Niarchos 2013) as input. Only the  $T_{\text{eff}}$  value of the primary component and the results of the  $v$ , analysis ( $\gamma$ ,  $e$ ,  $a$ ) were taken from our study and they were fixed during the analysis. The  $T_{\text{eff}}$  value of the primary star was found slightly different in two different approaches. Therefore, in this analysis, we used the average  $T_{\text{eff}}$  (7900 K) as input. The other fixed parameters are bolometric albedos (Ruciński 1969), bolometric gravity-darkening coefficient (von Zeipel 1924), and logarithmic limb darkening coefficient (van Hamme 1993). The TESS passband is not incorporated into the Wilson–Devinney code; therefore, the Cousins  $I_c$ -band was assumed in the binary modelling as the TESS passband is centred at Cousins  $I_c$ -band. The fixed coefficients were also chosen considering the  $I_c$ -band. Those coefficients were taken with the same way as given Kahraman Aliçavuş & Aliçavuş (2019). The  $T_{\text{eff}}$  of the cool component, phase shift ( $\phi$ ), orbital inclination ( $i$ ), possible third body light contribution ( $l_3$ ), the mass ratio ( $q = M_{\text{hot}}/M_{\text{cool}}$ ), fractional luminosities and the dimensionless potential ( $\Omega$ ) of binary components were used as free parameters. During the analysis, a semidetached binary configuration was assumed as the TZ Dra system has been classified as such before (Liakos & Niarchos 2013). The Wilson–Devinney code combined with Monte Carlo simulation was used in the binary modelling (Zola et al. 2004, 2010). As the system is an Algol-type binary, there could be mass transfer between the components which was shown by Liakos & Niarchos (2013). During mass transfers/losses, angular momentum changes and the velocity of the components might change. Therefore, we carried out the modelling by testing non-synchronous and synchronous rotation. As we obtained the better  $\chi^2$

<sup>4</sup>kurucz.harvard.edu/linelists.html

<sup>5</sup>First 10 highest amplitude frequencies given in Table 6.

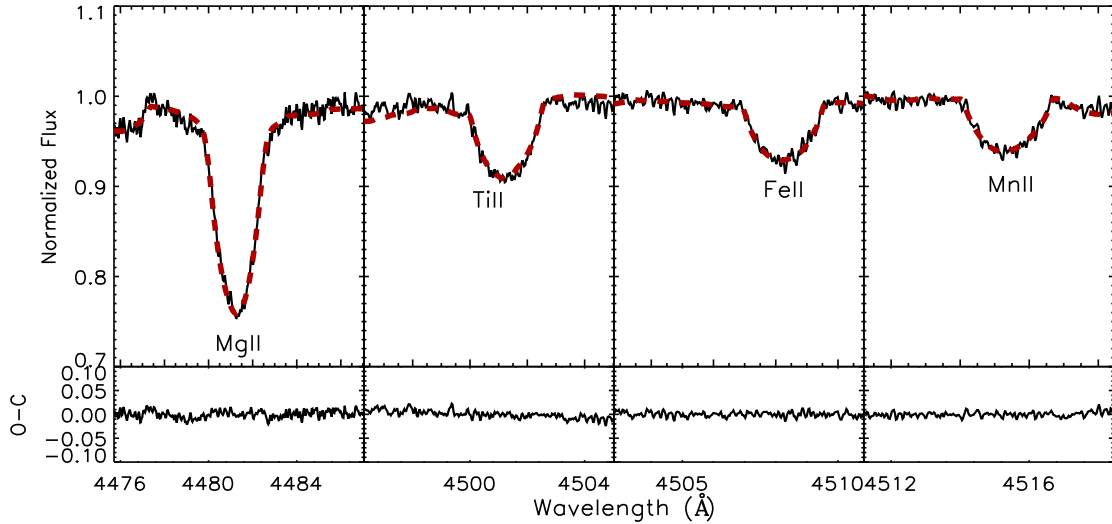


**Figure 4.** Consistency between the synthetic (dashed lines) and the observed spectra.

value for the synchronous rotation we worked with this assumption throughout the binary modelling.

As the system was found to be a single-lined binary, there is no certain information about the  $q$  value. Therefore, a  $q$  search was carried out by checking the minimum  $\chi^2$  value. Consequently, it was found that the  $q$  value should be around  $0.42 \pm 0.05$ . The  $q$  search is shown in Fig. A1. The binary modelling was started adopting  $q$  value input. In the first binary modelling steps, we noticed that in the out of eclipse light curve there are some asymmetries that are probably caused by a star-spot(s). Therefore, we included star-spot modelling in our analysis as well. As a result of this analysis, we found the best-fitting model with a hotspot on the primary star. The results of the binary modelling are listed in Table 4 and the best-fitting theoretical model to the *TESS* data is illustrated in Fig. 5. The Roche lobe geometry of the system with the hotspot on primary's surface is shown in Fig. 6

The fundamental stellar parameters such as  $M$ ,  $R$ , luminosity ( $L$ ), bolometric magnitude ( $M_{\text{bol}}$ ), absolute magnitude ( $M_V$ ), and also  $\log g$  parameters for both binary components were calculated using the mass function  $f$  found in the  $v_r$  analysis, the well-known Kepler and Pogson equations. These parameters are also listed in Table 4.

## 6 H $\alpha$ LINE PROFILE AND MASS TRANSFER EXAMINATION

Algols are semidetached, close, short-period binary systems that consist of a hot (B-A) main-sequence and a cooler, less massive evolved component. This evolved cooler component fills its Roche lobe and transfers mass from Roche lobe overflow (Kopal 1955). The mass transfer can be noticed from some additional features affecting the photometric and spectroscopic data. The effect of mass transfer in Algols shows itself especially as distortions in the  $v_r$  data of the primary component, and additional emission and/or absorption in the H  $\alpha$  and H  $\beta$  lines (Vesper et al. 2001; Soydugan et al. 2007). When the  $v_r$  curve, H  $\alpha$  and H  $\beta$  line profiles of TZ Dra were examined, we noticed a small distortion in the  $v_r$  data especially at around 0.75 phase and significantly different profile in H  $\alpha$ . As explained by Vesper et al. (2001), emissions are caused by stream-disc or star-stream interaction in a region between binary components. Absorption lines may also originate from the matter around the primary component or 'stream projected against primary'

**Table 4.** Results of the light curve analysis and the fundamental stellar parameters. Subscripts 1, 2, and 3 represent the primary, the secondary, and third binary components, respectively. <sup>a</sup> shows the Fixed Parameters.

Parameter	Value
$i$ ( $^\circ$ )	$75.138 \pm 0.015$
$T_1^a$ (K)	$7900 \pm 250$
$T_2$ (K)	$4970 \pm 233$
$\Omega_1$	$3.848 \pm 0.046$
$\Omega_2$	$2.734 \pm 0.035$
Phase shift	$-0.0044 \pm 0.0001$
$q$	$0.428 \pm 0.013$
$r_1^*$ (mean)	$0.2953 \pm 0.0036$
$r_2^*$ (mean)	$0.3070 \pm 0.0026$
$l_1 / (l_1 + l_2)$	$0.787 \pm 0.016$
$l_2 / (l_1 + l_2)$	$0.213 \pm 0.016$
$l_3$	0.0
Spot Parameters	
Co-Latitude (deg)	$90^a$
Longitude (deg)	$190.84 \pm 0.14$
Radius (deg)	$19.53 \pm 0.04$
Temperature Factor**	$1.052 \pm 0.012$
Derived Quantities	
$M_1$ ( $M_\odot$ )	$2.039 \pm 0.004$
$M_2$ ( $M_\odot$ )	$0.872 \pm 0.003$
$R_1$ ( $R_\odot$ )	$1.611 \pm 0.052$
$R_2$ ( $R_\odot$ )	$1.675 \pm 0.038$
$\log(L_1/L_\odot)$	$0.960 \pm 0.033$
$\log(L_2/L_\odot)$	$0.188 \pm 0.054$
$\log g_1$ (cgs)	$4.30 \pm 0.02$
$\log g_2$ (cgs)	$3.92 \pm 0.03$
$M_{\text{bol}1}$ (mag)	$2.34 \pm 0.07$
$M_{\text{bol}2}$ (mag)	$4.27 \pm 0.08$
$M_{V1}$ (mag)	$2.32 \pm 0.09$
$M_{V2}$ (mag)	$4.50 \pm 0.13$
$M_{\text{TESS}1}$ (mag)	$2.35 \pm 0.05$
$M_{\text{TESS}2}$ (mag)	$3.77 \pm 0.09$

\*Fractional radii, \*\* $T_{\text{eff,spot}}/T_{\text{eff,star}}$

(Vesper et al. 2001). Therefore, the existence of these absorption and emission profiles in H  $\alpha$  gives us information about the mass transfer. Consequently, we extracted the H  $\alpha$  line profiles of TZ Dra.

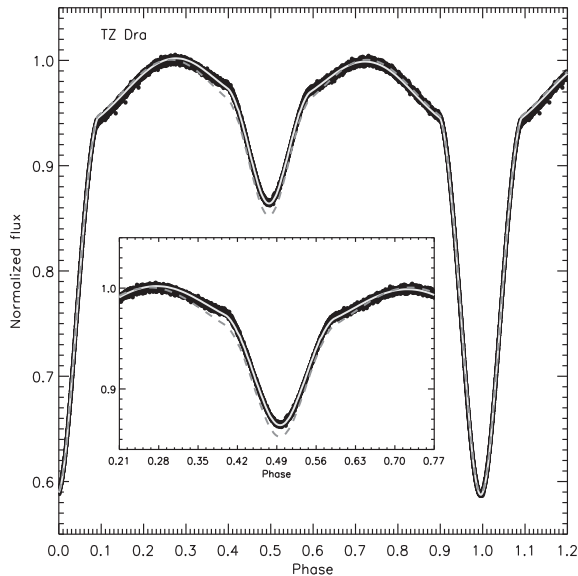


**Figure 5.** Theoretical binary modelling fit with spot assumption (solid line) and without spot assumption (dashed line).

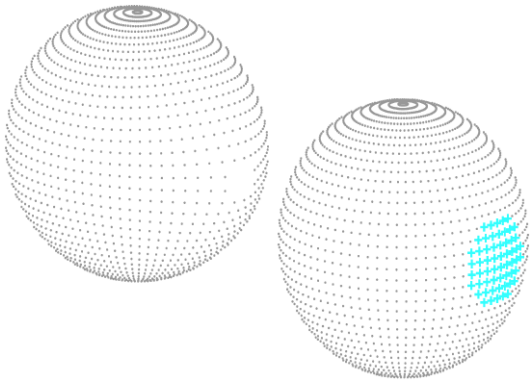


**Figure 6.** Roche geometry of TZ Dra at around 0.6 phase. Blue spot on the primary star represents the hotspot.

The best-fitting theoretical atmosphere model obtained in the analysis of the hydrogen lines was used in this analysis. This atmosphere model was fitted to the  $H\alpha$  profiles and then it was extracted from the observed  $H\alpha$  lines. In this way, the profiles of absorption and emission lines were obtained as shown in Fig. 7. In these residual spectra, we found one emission and two absorption line profiles. The  $v_r$  changes of these lines were measured and the variation of them according to the orbital phase were obtained as shown in Fig. 8. When the  $v_r$  variation of these lines was examined, we noticed that the profile of emission is caused by the star-stream or star-disc interaction between two stars. These interactions create emission lines and they are visible at around near quadrature phases as obtained in this study (Vesper et al. 2001). The absorption line 1 (see Fig. 7) is thought to be due to the stream projected against the primary component. In this case, absorption lines are observed near primary eclipse ingress or egress (Vesper et al. 2001) as we obtained for absorption line 1. Additionally, the  $v_r$  variations of this line follow the  $v_r$  profiles of the primary component. The other absorption line (line 2) seems to follow the secondary component and there is no explanation for this kind of absorption line profile occurring in Algol type systems. One interpretation could be that this line is caused

by the mass stream from the secondary component. It only detected around the primary eclipse as can be seen from Fig. 8. As a result, with this investigation, we revealed the mass transfer signature of TZ Dra.

## 7 ORBITAL PERIOD VARIATION

Mass transfer and mass-loss in a system can be evidenced by an orbital period variation analysis as well. Hence, we also studied the orbital period changes. All available literature minima times of TZ Dra were collected from the O-C Gateway.<sup>6</sup> Additionally, we used *TESS* data to calculate new minima times. In this calculation, only the SC data were used because the sampling of these light curves allows precise determination of the times of minima. We measured three primary and secondary minima times from each sector and in total 12 new minima times were derived from the *TESS* observations. To obtain a new minima time a photometric observation was carried out at the Çanakkale Onsekiz Mart Observatory with the IST60 telescope (60-cm). The minima times from the *TESS* and new photometric observation were calculated using the method of Kwee & van Woerden (1956). All the minima times are listed in Table A2. To increase the sensitivity of our orbital-period variation (O-C) analysis, in addition to *TESS* and new minima times, we used only the literature CCD and photoelectric minima times in the analysis. In total, 16 photoelectric and 67 CCD minima times including the *TESS* minimas were used. During the analysis, data weights were taken as 3 for photoelectric data and 10 for CCD measurements and the weighted least-squares method was used (Zasche et al. 2009).

When we examined the O-C diagram of TZ Dra, we found a parabolic variation combined with another periodic change. First, a parabolic fit was applied to the O-C data. As a result, the quadratic term ( $Q$ ) was found to be  $-1.3265 \times 10^{-10}$  and a quadratic ephemeris was obtained as follows:

$$HJD(\text{Min}I) = 2452500.6419(5) + 0.8660316(8)E \\ - 1.3265 \cdot 10^{-10}(4) \cdot E^2$$

The parabolic variations in the O-C diagram could be caused by mass transfer between the binary component and/or mass-loss from the system. For TZ Dra a  $0.009 \text{ s yr}^{-1}$  decrease in the orbital period was obtained as given in Table 5. This shows us that the mass-loss is effective in TZ Dra. We calculated the mass-loss amount in the system considering equation (16) of Erdem & Öztürk (2014). This equation includes impacts such as dynamic and tidal effects. As a result, the mass-loss amount was obtained as given in Table 5.

After removing the parabolic fit from the O-C data, we obtained another variation in the residuals. For the variation in the residual O-C diagram the light-time effect or light-traveltime (LITE; Zasche et al. 2009) caused by a third body orbiting around the centre of mass (e.g. Pribulla et al. 2005; Erdem et al. 2011) was tested. The physical relation between the O-C and LITE was formalized by Irwin (1959) who described the time delay ( $\Delta T$ ) in the period with the semimajor axis ( $a$ ), speed of light ( $c$ ),  $i$ ,  $e$ , true anomaly ( $v$ ), and longitude of periastron ( $w$ ). The best theoretical fit representing this variation in the O-C diagram is obtained by the following equation:

$$HJD(\text{Min}I) = 2452500.6419(5) + 0.8660316(8)E \\ - 1.3265(4) \times 10^{-10} E^2 + \Delta T.$$

As a result, in the system we found a third component with a 45.8-yr orbital period and a maximum mass of  $0.17 \pm 0.03 M_{\odot}$  if it has an

<sup>6</sup><http://var2.astro.cz/ocgate/>

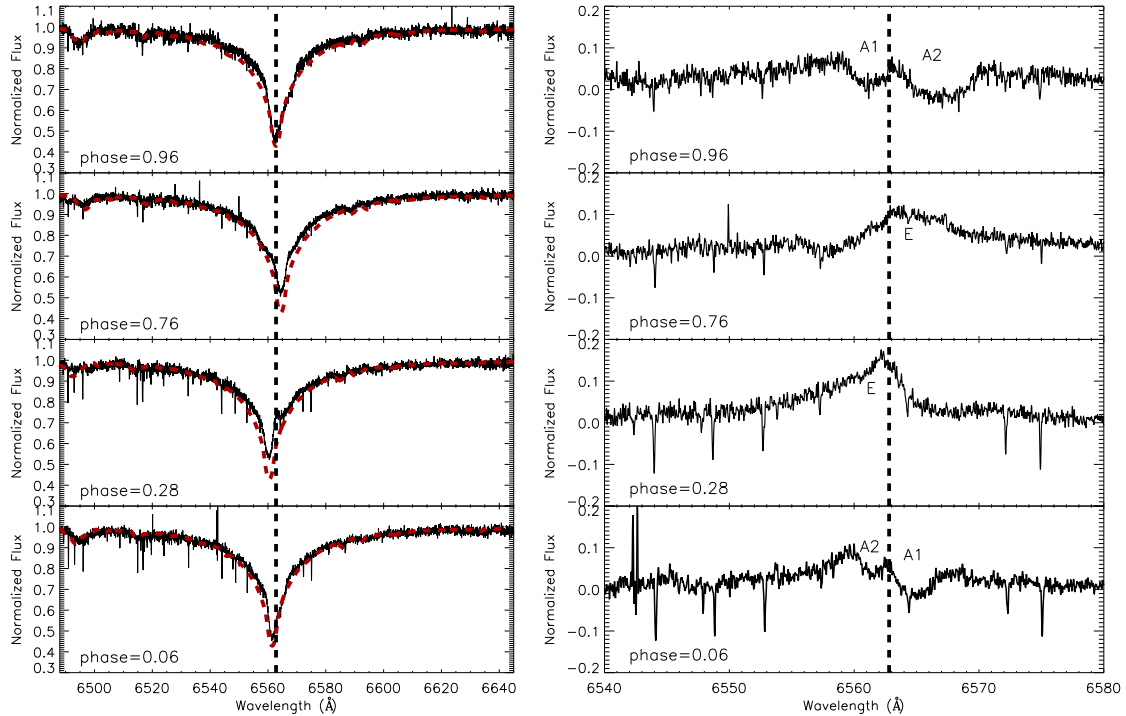


**Figure 7.** The H $\alpha$  profiles at different orbital phases (left-hand panels) and the residuals (right-hand panels) from the observed and the theoretical H $\alpha$  (red dashed lines) profiles shown in the left-hand panels. The vertical dashed lines represent the laboratory wavelength of H $\alpha$ . The abbreviations A1, A2, and E show absorption 1, absorption 2, and emission lines seen in the residuals.

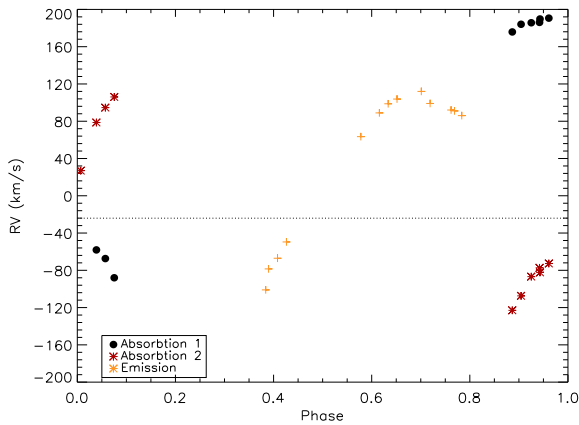


**Figure 8.** The radial velocity variations of the absorption and emission lines shown in Fig. 7.

orbital inclination of  $90^\circ$ . This third component could not be found in the binary modelling because of its relatively small mass. The results of the O-C analyses for the parabolic and LITE variations and the combined best theoretical fit to the observations are given in Table 5 and the best theoretical O-C fit to the observation points is shown in Fig. 9, respectively.

## 8 TIME-SERIES ANALYSIS

The effect of binary interaction on the pulsations of a pulsating mass-accreting Algol-type system, U Gru was discussed by Bowman et al. (2019). They show how important such systems are to probe the binary interaction with tidal asteroseismology. The possible effect of binary interactions and mass-transfer would change the structure and

**Table 5.** The results of the O-C diagram analysis. A and subscript 3 represent the amplitude of LITE and third body.

Parameter	Value
$T_0$ (HJD)	$2452500.6419 \pm 0.0005$
$P$ (day)	$0.86603164 \pm 0.00000008$
$Q$ (day). ( $10^{-10}$ )	$-1.3265 \pm 0.0003$
$dP/dT$ ( $s \text{ yr}^{-1}$ )	$-0.009 \pm 0.001$
$dM/dt$ ( $M_\odot \text{ yr}^{-1}$ ). $10^{-9}$	$-3.52 \pm 0.24$
$P_3$ (yr)	$45.82 \pm 0.90$
$a_3 \sin i$ (au)	$0.98 \pm 0.09$
$A_s$ (day)	$0.0032 \pm 0.0004$
$e_3$	$0.83 \pm 0.05$
$\omega_3$ (deg)	$170 \pm 7$
$f$ ( $m_3$ ) ( $M_\odot$ )	$0.0005 \pm 0.0001$
$m_3$ ( $M_\odot$ ) ( $i = 90$ )	$0.17 \pm 0.03$

evolution scenario of the pulsating component and these are missing in the stellar models. Therefore, such systems are valuable for the theoretical modelling of mass transfer effect and/or mass-loss effect on pulsations. Hence, we carried out a frequency analysis of TZ Dra system.

To perform a frequency analysis of the stellar pulsations we removed the mean binarity-induced light variations by a phenomenological fit consisting of the orbital frequency derived to be  $1.1547060 \pm 0.0000004 \text{ d}^{-1}$  from the *TESS* photometry alone and its first 100 harmonics.

The residuals after the fit were then searched for frequencies of pulsation using the PERIOD04 software (Lenz & Breger 2005). This package applies single-frequency power spectrum analysis and simultaneous multifrequency sine-wave fitting. It also includes advanced options such as the calculation of optimal light-curve

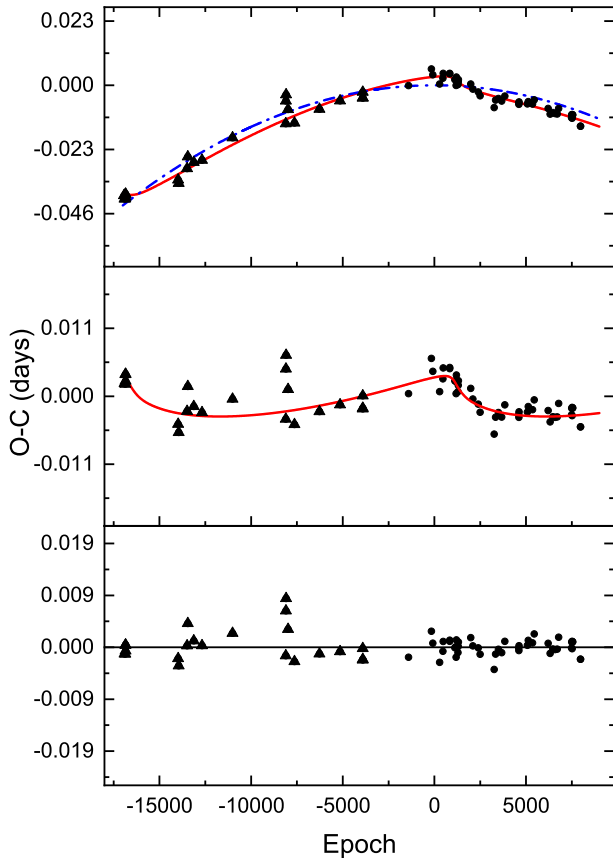


**Figure 9.** The theoretical fits to the O-C data. The upper panel shows both the parabolic (blue dashed line) and the parabolic plus LITE model fit (red). The middle and lower panels illustrate the LITE fit alone and the residuals from the combined fit, respectively. The triangle and circle symbols represent the photoelectric and CCD data, respectively.

fits for multiperiodic signals including harmonic, combination, and equally spaced frequencies. These sine-wave fits are subtracted from the data and the residuals examined for the presence of further periodicities. The application of this procedure, called pre-whitening, to TZ Dra is illustrated in Fig. 10.

To decide whether or not a periodic signal in a time-series is statistically significant or not, several criteria have been proposed, the most commonly used probably the one by Breger et al. (1993). This criterion states that a given peak must exceed the mean amplitude in the Fourier spectrum by a factor of 4 in the local frequency domain to be considered significant. For space-based data, this can, however, lead to an overinterpretation of the periodic content (Balona 2014). Consequently, we have stopped the frequency search after the detection of 35 pulsational signals to err on the side of caution; the strongest residual peak in the lowest panels of Fig. 10 has an amplitude S/N ratio of 4.4, with the noise calculated in a  $10 \text{ d}^{-1}$  window centred around it.

During the frequency analysis it became clear that many of the pulsational signals are spaced by integer multiples of the orbital frequency  $\nu_{\text{orb}}$  from other pulsation frequencies. We therefore required that PERIOD04 would fix those frequencies to exactly the predicted value as the orbital frequency is determined to considerably higher precision than the individual pulsation frequencies. We list the frequency solution so derived in Table 6, where we also quote formal errors on the derived parameters following Montgomery & Odonoghue (1999).

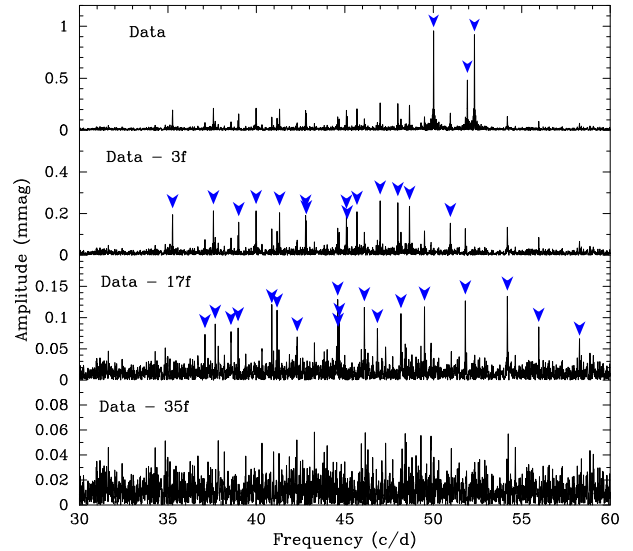


**Figure 10.** The Fourier Transform of the residual *TESS* light curve of TZ Dra after filtering the binarity-induced light variations (top) and subsequent pre-whitening steps. The blue arrows denote the signals detected.

**Table 6.** A least-squares fit of the pulsation frequencies of TZ Dra. The zero-point for the phases,  $t_0 = 2459008.8585$ , has been chosen to be at a time of primary eclipse. Error estimates for the independent frequencies and phases are given in braces in units of the last digits after the comma.

	Frequency $\text{d}^{-1}$	Amplitude mmag $\pm 0.012$	Phase radians
$\nu_1$	50.0174(1)	0.950	4.51(1)
$\nu_1 + 2\nu_{\text{orb}}$	52.3268(1)	0.910	1.35(1)
$\nu_2$	51.9264(2)	0.467	0.83(2)
$\nu_3 - 2\nu_{\text{orb}}$	44.6863(12)	0.092	1.84(11)
$\nu_3$	46.9957(4)	0.264	4.95(4)
$\nu_4 - \nu_{\text{orb}}$	45.6875(5)	0.212	3.73(5)
$\nu_4$	46.8422(13)	0.082	3.42(12)
$\nu_4 + \nu_{\text{orb}}$	47.9969(4)	0.254	3.73(4)
$\nu_5$	48.6545(5)	0.235	4.91(4)
$\nu_5 + 2\nu_{\text{orb}}$	50.9639(7)	0.154	1.88(7)
$\nu_6$	37.5715(5)	0.218	3.16(5)
$\nu_6 - 2\nu_{\text{orb}}$	35.2621(6)	0.195	3.06(5)
$\nu_7$	41.3112(5)	0.207	4.71(5)
$\nu_7 - 2\nu_{\text{orb}}$	39.0018(7)	0.149	4.86(7)
$\nu_8$	39.9832(5)	0.214	6.26(5)
$\nu_8 - 2\nu_{\text{orb}}$	37.6738(12)	0.089	3.00(11)
$\nu_9$	45.0894(6)	0.194	1.75(5)
$\nu_9 - 2\nu_{\text{orb}}$	42.7800(6)	0.190	4.88(5)
$\nu_{10}$	42.8204(7)	0.167	2.88(6)
$\nu_{10} + 2\nu_{\text{orb}}$	45.1298(8)	0.139	6.15(7)
$\nu_{11}$	51.8128(9)	0.128	4.10(8)
$\nu_{11} - 2\nu_{\text{orb}}$	49.5034(9)	0.118	4.21(9)
$\nu_{12}$	54.1882(8)	0.134	4.86(8)
$\nu_{12} - 7\nu_{\text{orb}}$	46.1053(9)	0.117	1.66(9)
$\nu_{13}$	40.8723(10)	0.114	4.03(9)
$\nu_{13} - 2\nu_{\text{orb}}$	38.5629(14)	0.079	4.25(13)
$\nu_{14}$	58.2668(18)	0.062	2.87(16)
$\nu_{14} - 2\nu_{\text{orb}}$	55.9574(13)	0.084	5.81(12)
$\nu_{15}$	44.6175(14)	0.076	3.90(13)
$\nu_{15} - 2\nu_{\text{orb}}$	42.3081(16)	0.069	4.14(15)
$\nu_{16}$	44.5955(9)	0.126	2.23(8)
$\nu_{17}$	41.1696(10)	0.107	2.44(10)
$\nu_{18}$	48.1700(10)	0.106	4.19(10)
$\nu_{19}$	38.9667(13)	0.085	2.53(12)
$\nu_{20}$	37.0940(15)	0.074	1.21(14)



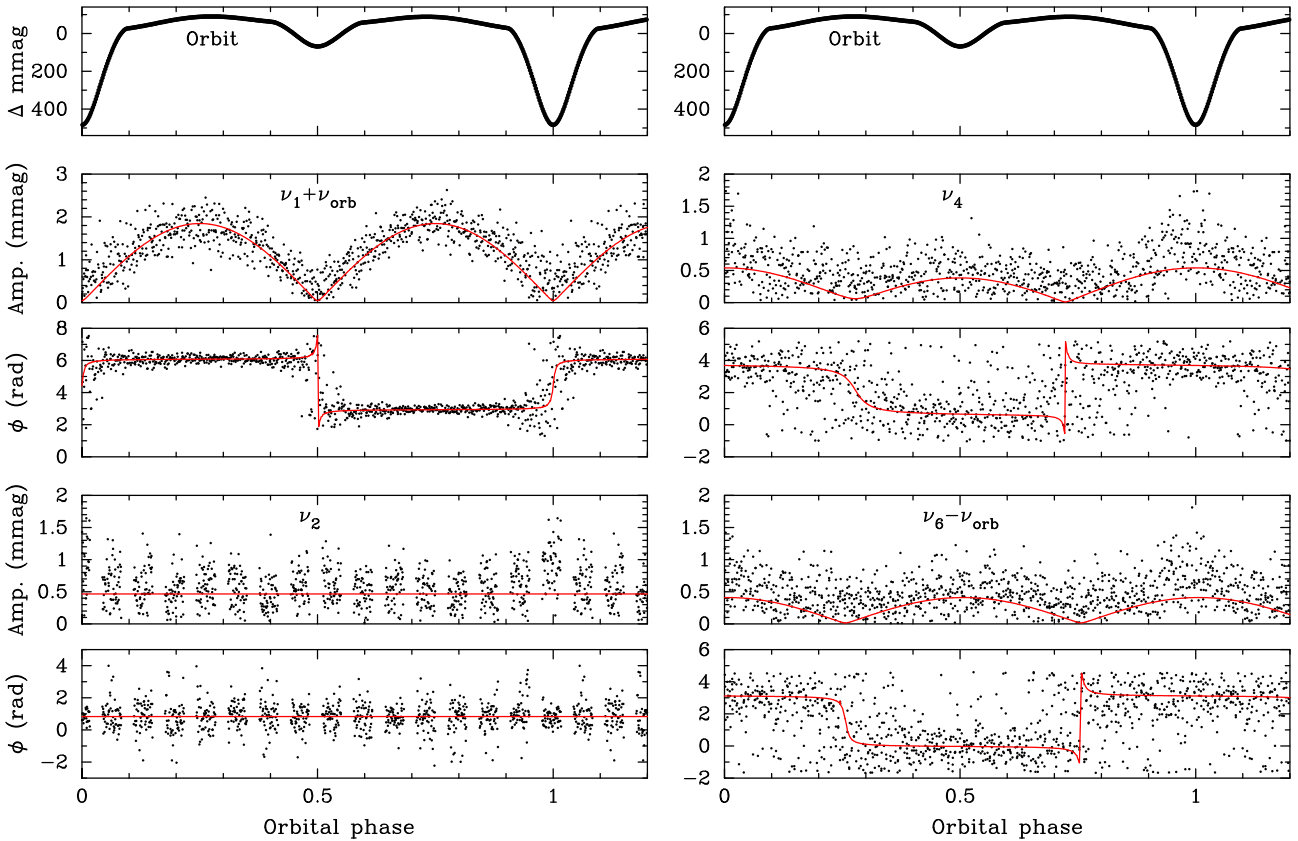


**Figure 11.** The run of the pulsation amplitudes and phases of four selected modes of TZ Dra over the orbital cycle (bottom four panels left and right). The black dots are individual determinations, the red lines are fits using the signal parameters from Table 6. Top: binary-induced light curve.

The pulsation frequencies determined this way range from 35.26 to 58.27 d<sup>-1</sup>. From the mass and radius for the primary  $\delta$  Scuti pulsator, one can derive pulsation ‘constants’  $Q_i = P_i \sqrt{(\rho/\rho_\odot)}$ <sup>7</sup> between 0.012 and 0.020 d. This corresponds to pulsation in relatively high-order  $p$  modes in the range of the second to fifth radial overtone (Fitch 1981) which, in combination with the relatively unevolved state of the pulsator, leads to the expectation of a pulsation spectrum with regular frequency structures.

14 out of the 20 independent pulsation frequencies detected for TZ Dra occur in multiplets. 12 of those are doublets spaced by twice the orbital frequency, one is a triplet with a weak centroid spaced by the orbital frequency. With one exception, all of the single frequencies are low in amplitude, so it is possible that they have undetected multiplet companions. Furthermore, many of the doublet components are fairly similar in amplitude, and all of them are, within the errors, either in phase or  $\pi$  rad out of phase at primary minimum.

These are signatures of tidally tilted pulsation. Reed, Brondel & Kawaler (2005) have shown how the oscillation spectrum of a single mode of given spherical degree  $l$  and azimuthal order  $m$  becomes modified due to the varying aspect of the pulsation axis over the orbital cycle. In brief, a single frequency splits up into multiplets determined by the type of mode, and by the inclination of the pulsational and rotational axes. These multiplets are spaced by integer multiples of the orbital frequency. This is what is seen here. The frequency doublets in our case thus are parts of multiplets

centred on the frequency average of the two components. In Fig. 11, we show the behaviour of the amplitudes and phases of a few selected modes over the orbit.

The amplitude of the  $\nu_1$  doublet is at maximum near quadrature, and reaches almost zero near primary and secondary eclipse, respectively. The zero-crossing means that a node line of a non-radial pulsation mode crosses the line of sight. Assuming that the pulsational axis lies in the orbital plane (there would be no amplitude modulation if it was aligned with the rotational axis which we assume to be normal to the orbital plane), this must therefore be a sectoral mode. The singlet  $\nu_2$  shows no phase modulation over the orbital cycle and almost no amplitude variation, except near primary eclipse. This would at first sight imply a radial mode. However, in that case one would expect the pulsation amplitude to decrease near primary eclipse, when part of the pulsating star is covered by the cooler companion that, at this orbital phase, contributes relatively more to the total flux observed. That this is not the case implies that  $\nu_2$  is also due to a non-radial mode, and that the increase in amplitude during primary eclipse is due to part of the surface that causes geometrical cancellation (Dziembowski 1977) being covered by the companion. The mode triplet  $\nu_4$  and the doublet including  $\nu_6$  behave similarly: they have highest amplitude at primary and secondary eclipse, respectively, but an amplitude close to zero near quadrature. They are therefore tidally tilted axisymmetric modes.

Which of the mode doublets correspond to axisymmetric and sectoral modes, respectively, can be directly read off Table 6. The multiplets that are in phase at primary minimum (triplet  $\nu_4$  and the doublets containing  $\nu_6, \nu_7, \nu_{11}, \nu_{13},$  and  $\nu_{15}$ ) are the  $m = 0$  modes and

<sup>7</sup> $P_i$ : Period of the used frequency.

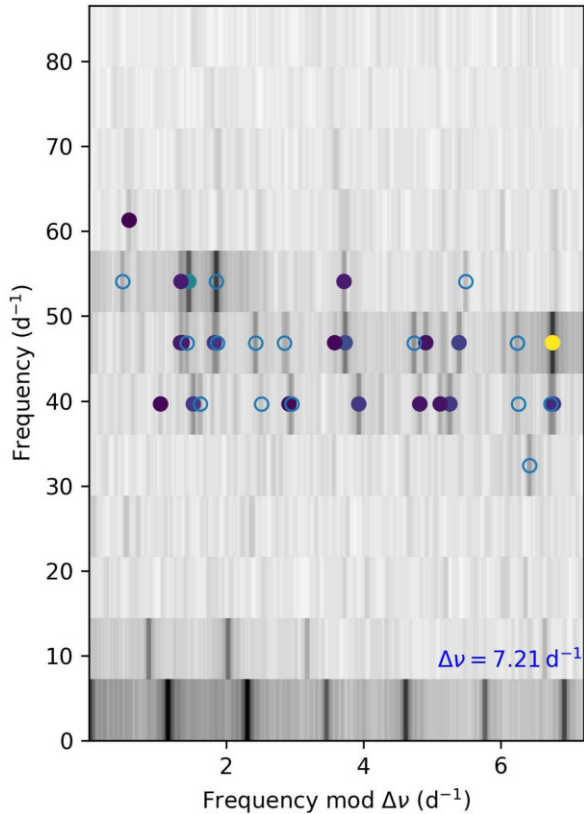


**Figure 12.** The grey-scale shows the Fourier amplitude spectrum of TZ Dra after removing the binary variations, shown in echelle format. The symbols show the peaks listed in Table 6, colour-coded by amplitude. The open symbols are marked in Table 6 as being combinations with the orbital frequency. The figure was produced using the *echelle* package (Hey & Ball 2020).

the doublets  $\pi$  rad out of phase ( $\nu_1, \nu_3, \nu_5, \nu_8, \nu_9, \nu_{10}, \nu_{12}$ , and  $\nu_{14}$ ) are sectoral modes. It is interesting to note that the centroid frequencies of the doublets containing axisymmetric modes are fairly equally spaced in frequency and may imply a mean frequency spacing of about  $7.1 \text{ d}^{-1}$  for consecutive radial orders of modes of the same  $l$ , which is close to the expected value of a star with the parameters of the primary of TZ Dra listed in Table 4. Whereas a detailed seismic study of the pulsating component of TZ Dra is out of the scope of this paper, and will need proper consideration of the tidal distortion of the oscillations (cf. Fuller et al. 2020) and the altered stellar structure due to ongoing mass transfer (e.g. Miszuda, Szewczuk & Daszyńska-Daszkiewicz 2021), let it suffice to say that this is a very interesting system for more in-depth theoretical modelling.

In comparison to the remaining pulsational mode structure of TZ Dra, the frequency doublet  $\nu_{12}$  and  $\nu_{12} - 7\nu_{\text{orb}}$  appears to be an ‘outlier’. Perhaps the frequency match is just a numerical agreement, but in that case there would be little reason why the phases of those two signals are also  $\pi$  rad out of phase. This is a hint that these two signals are generated by the same pulsation mode, which then must, however, be  $l > 3$ .

The pattern of high-frequency pulsation modes in TZ Dra is similar to those found in young delta Scuti stars by Bedding et al. (2020). In Fig. 12, we show the Fourier amplitude spectrum of TZ Dra in échelle format, using the residual light curve after removing the binary signal. Using a large separation of  $\Delta\nu = 7.21 \text{ d}^{-1}$ , we see that the pulsation modes align in several vertical ridges, similar to the

examples of more complicated echelle diagrams in fig. 4 of Bedding et al. (2020).

## 9 DISCUSSION AND CONCLUSIONS

In this study, we present the results of the spectroscopic and *TESS* photometric examinations of TZ Dra. Using the high-resolution spectra, we measured the radial velocities of primary component and found no significant signal from the cool (secondary) component. Therefore, the spectral analysis was carried out only for the hot (primary) component. The *TESS* photometric data were used in the binary modelling and pulsational frequency analysis.

The first binary modelling of the system was performed by Liakos & Niarchos (2013). Since they used ground-based photometric data in their analysis, there are significant differences between the results of our binary modelling and theirs because of the sensitivity difference between the *TESS* and ground-based data. The  $i$  ( $77.6^\circ$ ) and  $q$  (0.31) values show significant discrepancy, as a result the fundamental stellar parameters obtained in this study are quite different from the findings of Liakos & Niarchos (2013). Additionally, in their analysis, no spot variation was found in the light curve. Thanks to the spectroscopic measurements and high-quality *TESS* data the fundamental stellar parameters for TZ Dra system were determined precisely.

TZ Dra is an Algol-type system. In such semidetached systems, it is known that the mass transfers from the evolved cool component to the hot primary component. The effects of this mass transfer can be seen in the photometric and spectroscopic data. Therefore, we traced the signature of mass transfer especially in the spectra of TZ Dra. It turned out that  $H\alpha$  lines show quite different structures which allowed us to confirm the mass transfer. As a result of the  $H\alpha$  line profile, we found that there is an emission line that is caused by the star-stream or star-disc interaction between both binary components. Additionally, it was obtained that there is a stream projected against the hot component. Furthermore, in the binary modelling, we also found a hotspot on the primary star’s surface.

To explain the mass-loss in Algol-type systems there are four different mechanisms, bipolar jets (Umana et al. 2000; Umana, Leone & Trigilio 2002), mass-loss from the third Lagrangian point (Syrov et al. 2007), winds (Maeder & Stahler 2009), and the presence of a hotspot (Deschamps et al. 2013, 2015). The hotspot mechanism seems to be the more suitable and convincing mechanism to explain mass-loss from Algols. According to the hotspot model, the mass should be ejected from the primary star’s surface via the radiation pressure of the hotspot (van Rensbergen et al. 2011; Deschamps et al. 2013, 2015). To reveal possible mass-loss from the system an orbital period variation analysis was performed as well. In conclusion, a decrease in the orbital period was obtained and that could be explained with the mass-loss via the hotspot and the winds in the secondary component. With these results, we showed that TZ Dra is an important system to understand the mass transfer and the mass-loss mechanism in Algol-type binaries.

The pulsation feature of the primary binary component was examined and high pulsation frequencies (i.e.  $p$  modes) ranging from  $35.26$  to  $58.27 \text{ d}^{-1}$  were found. During the analysis, it was found that significant amount of pulsation frequencies are spaced by integer multiples of the orbital frequency and the star was shown to be a tidally tilted pulsator. According to the pulsation analysis, we estimated that the star show high-order  $p$  modes in the range of second to fifth radial overtones. Good evidence for a regular

pulsational frequency spacing of about  $7.2 \text{ d}^{-1}$  was found both from the tidally tilted pulsations and an échelle diagram.

TZ Dra is an interesting object for understanding the mass transfer and mass-loss mechanism in Algol-type systems, as well as its impact on the pulsations. With the combination of the results of the studies for similar systems, these effects can be interpreted more efficiently and help us improve the current knowledge about the Algol type pulsating systems.

## ACKNOWLEDGEMENTS

The authors would like to thank the reviewer for useful comments and suggestions that helped to improve the publication. This study has been supported by the Scientific and Technological Research Council (TUBITAK) project through 120F330. GH thanks the Polish National Center for Science (NCN) for supporting the study through grant 2015/18/A/ST9/00578. IST60 telescope and its equipment are supported by the Republic of Turkey Office of Strategy and Budget with the project 2016K12137 and Istanbul University with the project numbers BAP-3685 and FBG-2017-23943. TRB acknowledges support from the Australian Research Council through Discovery Project DP210103119. Based on observations made with the Mercator Telescope, operated on the island of La Palma by the Flemish Community, at the Spanish Observatorio del Roque de los Muchachos of the Instituto de Astrofísica de Canarias. The *TESS* data presented in this paper were obtained from the Mikulski Archive for Space Telescopes (MAST). Funding for the *TESS* mission is provided by the NASA Explorer Program. This work has made use of data from the European Space Agency (ESA) mission *Gaia* (<http://www.cosmos.esa.int/gaia>), processed by the *Gaia* Data Processing and Analysis Consortium (DPAC, <http://www.cosmos.esa.int/web/gaia/dpac/consortium>). Funding for the DPAC has been provided by national institutions, in particular the institutions participating in the *Gaia* Multilateral Agreement. This research has made use of the SIMBAD data base, operated at CDS, Strasbourg, France.

## DATA AVAILABILITY

The data underlying this work will be shared at reasonable request to the corresponding author.

## REFERENCES

- Alfonso-Garzón J., Montesinos B., Moya A., Mas-Hesse J. M., Martín-Ruiz S., 2014, *MNRAS*, 443, 3022
- Asplund M., Grevesse N., Sauval A. J., Scott P., 2009, *ARA&A*, 47, 481
- Baglin A. et al., 2006, 36th COSPAR Scientific Assembly, meeting abstract from the CDROM, #3749
- Baker N., Kippenhahn R., 1962, *Z. Astrophys.*, 54, 114
- Balona L. A., 2014, *MNRAS*, 439, 3453
- Balona L. A., Dziembowski W. A., 2011, *MNRAS*, 417, 591
- Bedding T. R. et al., 2020, *Nature*, 581, 147
- Borucki W. J. et al., 2010, *Science*, 327, 977
- Bowman D. M., Kurtz D. W., 2018, *MNRAS*, 476, 3169
- Bowman D. M., Johnston C., Tkachenko A., Mkrтчichian D. E., Gunsriwaw K., Aerts C., 2019, *ApJ*, 883, L26
- Breger M., 2000, in Breger M., Montgomery M., eds, ASP Conf. Ser. Vol. 210, Delta Scuti and Related Stars. Astron. Soc. Pac., San Francisco, p. 3
- Breger M. et al., 1993, *A&A*, 271, 482
- Brogliá P., Conconi P., 1984, *A&A*, 138, 443
- Catanzaro G., Leone F., Dall T. H., 2004, *A&A*, 425, 641
- da Silva R., Maceroni C., Gandolfi D., Lehmann H., Hatzes A. P., 2014, *A&A*, 565, A55
- Deschamps R., Siess L., Davis P. J., Jorissen A., 2013, *A&A*, 557, A40
- Deschamps R., Braun K., Jorissen A., Siess L., Baes M., Camps P., 2015, *A&A*, 577, A55
- Dziembowski W., 1977, *Acta Astron.*, 27, 203
- Erdem A., Öztürk O., 2014, *MNRAS*, 441, 1166
- Erdem A., Aliçavuş F., Soyduğan F., Dođru S. S., Soyduğan E., Çiçek C., Demircan O., 2011, *New Astron.*, 16, 498
- Faulkner D. R., 1986, *PASP*, 98, 690
- Fitch W. S., 1981, *ApJ*, 249, 218
- Fuller J., Kurtz D. W., Handler G., Rappaport S., 2020, *MNRAS*, 498, 5730
- Handler G. et al., 2020, *Nat. Astron.*, 4, 684
- Herbig G. H., 1960, *ApJ*, 131, 632
- Hey D., Ball W., 2020, *Zenodo*
- Irwin J. B., 1959, *AJ*, 64, 149
- Joergensen H. E., Gronbech B., 1978, *A&A*, 66, 377
- Kahraman Aliçavuş F., Aliçavuş F., 2020, *MNRAS*, 488, 5279
- Kahraman Aliçavuş F. et al., 2016, *MNRAS*, 458, 2307
- Kahraman Aliçavuş F., Soyduğan E., Smalley B., Kubát J., 2017, *MNRAS*, 470, 915
- Kopal Z., 1955, *Ann. Astrophys.*, 18, 379
- Kreiner J. M., 2004, *Acta Astron.*, 54, 207
- Kurtz D. W. et al., 2020, *MNRAS*, 494, 5118
- Kurucz R., 1993, KurCD, ATLAS9 Stellar Atmosphere Programs and 2 km/s grid. Kurucz CD-ROM No. 13. Cambridge, 13
- Kurucz R. L., Avrett E. H., 1981, *SAO Special Report #391*
- Kwee K. K., van Woerden H., 1956, *Bull. Astron. Inst. Neth.*, 12, 327
- Lampens P., 2021, *Galaxies*, 9, 28
- Lenz P., Breger M., 2005, *Commun. Asteroseismology*, 146, 53
- Liakos A., Niarchos P., 2013, *Ap&SS*, 343, 123
- Liakos A., Niarchos P., 2017, *MNRAS*, 465, 1181
- Maeder A., Stahler S., 2009, *Physics Today*, 62, 52
- Miszuda A., Szewczuk W., Daszyńska-Daszkiewicz J., 2021, *MNRAS*, 505, 3206
- Mkrтчichian D. E. et al., 2002, in Sterken C., Kurtz D. W., eds, ASP Conf. Ser. Vol. 256, Observational Aspects of Pulsating B- and A Stars. Astron. Soc. Pac., San Francisco, p. 259
- Mkrтчichian D. E. et al., 2004, *A&A*, 419, 1015
- Mkrтчichian D. E., Rodríguez E., Olson E. C., Kusakin A. V., Kim S.-L., Lehmann H., Gamarova A. Y., Kang Y. W., 2005, in Claret A., Giménez A., Zahn J.-P., eds, ASP Conf. Ser. Vol. 333, Tidal Evolution and Oscillations in Binary Stars: Third Granada Workshop on Stellar Structure. Astron. Soc. Pac., San Francisco, p. 197
- Moe M., Di Stefano R., 2017, *ApJS*, 230, 15
- Montgomery M. H., Odonoghue D., 1999, *Delta Scuti Star Newsletter*, 13, 28
- Murphy S. J., Hey D., Van Reeth T., Bedding T. R., 2019, *MNRAS*, 485, 2380
- Pribulla T., Chochol D., Tremko J., Kreiner J. M., 2005, in Sterken C., ed. ASP Conf. Ser. Vol. 335, The Light-Time Effect in Astrophysics. Astron. Soc. Pac., San Francisco, p. 103
- Rappaport S. A. et al., 2021, *MNRAS*, 503, 254
- Raskin G. et al., 2011, *A&A*, 526, A69
- Reed M. D., Brondel B. J., Kawaler S. D., 2005, *ApJ*, 634, 602
- Ricker G. R., et al., 2014, in Oschmann J. M., Clampin M., Fazio G. G., MacEwen H. A., eds, Proc. SPIE Conf. Ser. Vol. 9143, Space Telescopes and Instrumentation 2014: Optical, Infrared, and Millimeter Wave. SPIE, Bellingham, p. 914320
- Ricker G. R. et al., 2015, *J. Astron. Telesc. Instrum. Syst.*, 1, 014003
- Rodríguez E. et al., 2004, *MNRAS*, 347, 1317
- Ruciński S. M., 1969, *Acta Astron.*, 19, 245
- Sana H., Evans C. J., 2011, in Neiner C., Wade G., Meynet G., Peters G., eds, *Proc. IAU Symp. 272, Active OB stars: structure, evolution, mass loss, and critical limits*. p. 474
- Smalley B., 2005, *MSAIS*, 8, 130
- Smalley B., Gardiner R. B., Kupka F., Bessell M. S., 2002, *A&A*, 395, 601
- Southworth J., 2021, *Universe*, 7, 369
- Soyduğan E., Demircan O., Akan M. C., Soyduğan F., 2003, *AJ*, 126, 1933

- Soydugan E., Soydugan F., Demircan O., İbanoğlu C., 2006, *MNRAS*, 370, 2013
- Soydugan F., Frasca A., Soydugan E., Catalano S., Demircan O., İbanoğlu C., 2007, *MNRAS*, 379, 1533
- Soydugan E. et al., 2008, *Commun. Asteroseismology*, 157, 379
- Soydugan E., Soydugan F., Şenyüz T., Püsküllü Ç., Demircan O., 2011, *New Astron.*, 16, 72
- Steindl T., Zwintz K., Bowman D. M., 2021, *A&A*, 645, A119
- Sumter G. C., Beaky M. M., 2007, *Inf. Bull. Var. Stars*, 5798, 1
- Sytov A. Y., Kaigorodov P. V., Bisikalo D. V., Kuznetsov O. A., Boyarchuk A. A., 2007, *Astron. Rep.*, 51, 836
- Tempesti P., 1971, *Inf. Bull. Var. Stars*, 596, 1
- Tody D., 1986, in Crawford D. L., ed., *Proc. SPIE Conf. Ser. Vol. 627, Instrumentation in Astronomy VI*. SPIE, Bellingham, p. 733
- Umama G., Maxted P. F. L., Trigilio C., Fender R. P., Leone F., Yerli S. K., 2000, *A&A*, 358, 229
- Umama G., Leone F., Trigilio C., 2002, *A&A*, 391, 609
- van Hamme W., 1993, *AJ*, 106, 2096
- van Rensbergen W., de Greve J. P., Mennekens N., Jansen K., de Loore C., 2011, *A&A*, 528, A16
- Vesper D., Honeycutt K., Hunt T., 2001, *AJ*, 121, 2723
- von Zeipel H., 1924, *MNRAS*, 84, 665
- Wilson R. E., Devinney E. J., 1971, *ApJ*, 166, 605
- Zasche P., Liakos A., Niarchos P., Wolf M., Manimanis V., Gazeas K., 2009, *New Astron.*, 14, 121
- Zola S. et al., 2004, *Acta Astron.*, 54, 299
- Zola S., Gazeas K., Kreiner J. M., Ogloza W., Siwak M., Koziel-Wierzbowska D., Winiarski M., 2010, *MNRAS*, 408, 464

## APPENDIX A

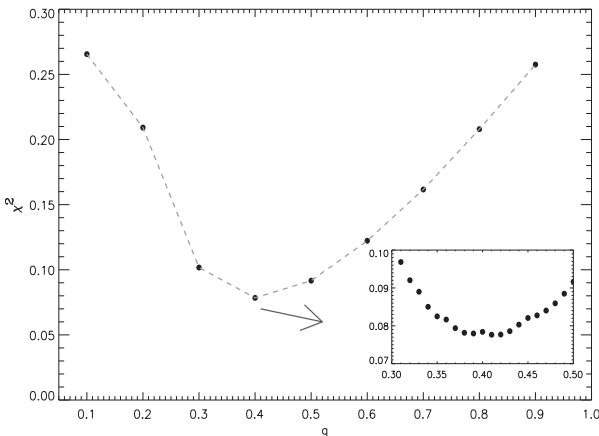


**Figure A1.**  $q$  search for TZ Dra.

**Table A1.** Values of the  $v_r$  measurements. The \* symbol shows the spectra used in the spectral analysis according to the orbital phase.

HJD (2450000 +)	phase	$v_r$ (km s <sup>-1</sup> )
8986.67841	0.39	-90.041 ± 0.327
8988.55955	0.56*	-11.297 ± 0.331
8990.68251	0.01	-48.080 ± 0.421
8996.64154	0.89	25.589 ± 0.472
9052.50644	0.39	-84.507 ± 0.377
9052.52226	0.41	-67.123 ± 0.357
9052.53807	0.43	-60.867 ± 0.511
9053.50377	0.54*	3.202 ± 0.513
9053.51966	0.56*	13.055 ± 0.314
9053.53540	0.58	18.949 ± 0.331
9053.55098	0.60	27.319 ± 0.327
9054.48047	0.67	59.870 ± 1.516
9054.50819	0.71	65.697 ± 1.313
9054.52371	0.72	66.848 ± 1.321
9054.55120	0.76	62.872 ± 1.490
9054.56680	0.77	61.067 ± 1.358
9055.53483	0.89	30.682 ± 0.500
9055.55030	0.91	18.770 ± 0.571
9055.56834	0.93	13.521 ± 0.536
9055.58374	0.95	8.488 ± 0.456
9055.59933	0.96	0.392 ± 0.492
9056.44893	0.94	11.107 ± 0.552
9058.47553	0.28	-111.006 ± 1.289
9059.46862	0.43	-56.888 ± 0.607
9060.45183	0.57	13.703 ± 0.637
9090.47989	0.24	-111.172 ± 0.503
9093.38956	0.60	33.861 ± 1.110
9093.40534	0.62	40.637 ± 1.308
9093.42083	0.63	46.740 ± 0.868
9093.43644	0.66	54.564 ± 0.921
9094.40102	0.77	67.568 ± 1.313
9094.41671	0.78	62.270 ± 1.219
9094.43230	0.80	60.672 ± 1.153
9096.36986	0.04	-49.920 ± 0.682
9096.38560	0.06	-55.208 ± 0.387
9096.40135	0.08	-61.628 ± 0.546

**Table A2.** The minima times derived from the *TESS* data and our photometric observation in V and R filter. I and II represent the primary and secondary minimums. For the V,R photometric observation a median minima time is given.

Time of minima HJD (2450000 +)	Filter	Minima type
8983.74370 ± 0.00003	<i>TESS</i>	I
8985.47575 ± 0.00002	<i>TESS</i>	I
9008.85843 ± 0.00003	<i>TESS</i>	I
8984.17794 ± 0.00011	<i>TESS</i>	II
8985.04381 ± 0.00020	<i>TESS</i>	II
9003.23004 ± 0.00008	<i>TESS</i>	II
9010.59182 ± 0.00003	<i>TESS</i>	I
9025.31420 ± 0.00004	<i>TESS</i>	I
9032.24248 ± 0.00003	<i>TESS</i>	I
9011.89158 ± 0.00010	<i>TESS</i>	II
9025.74788 ± 0.00009	<i>TESS</i>	II
9032.67621 ± 0.00009	<i>TESS</i>	II
9405.49803 ± 0.00029	VR	I

This paper has been typeset from a  $\text{\LaTeX}$  file prepared by the author.